Cell Reports

Article

Topology recapitulates morphogenesis of neuronal dendrites

Graphical abstract

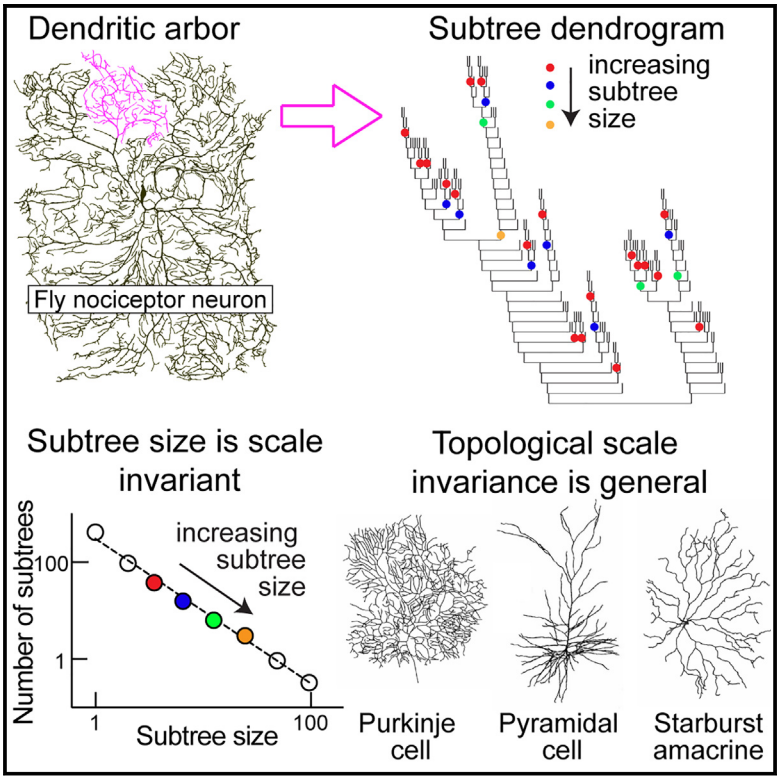

Highlights

- Neuronal cell types can be distinguished by the topologies of their dendritic arbors
- For many neurons, the distribution of subtree sizes is scale invariant
- Postsynaptic spines and branchlets cause deviations from scale invariance
- The subtree-size distribution reflects the underlying branching processes

Authors

Maijia Liao, Alex D. Bird, Hermann Cuntz, Jonathon Howard

Correspondence

joe.howard@yale.edu

In brief

Liao et al. found that the dendritic arbors of many neurons have topological scale invariance: the distributions of subtree sizes follow power laws. Simulations indicate that scale invariance arises from repetitive application of branching rules, including those that optimally balance material costs and conduction times.

Liao et al., 2023, Cell Reports *42*, 113268
November 28, 2023
https://doi.org/10.1016/j.celrep.2023.113268

CellPress

Cell Reports

CellPress
OPEN ACCESS

Article

Topology recapitulates morphogenesis of neuronal dendrites

Maijia Liao,[1] Alex D. Bird,[2,3] Hermann Cuntz,[2,3] and Jonathon Howard[1,4,*]
[1]Department of Molecular Biophysics & Biochemistry, Yale University, New Haven, CT 06520, USA
[2]Ernst Strüngmann Institute (ESI) for Neuroscience in Cooperation with Max Planck Society, 60528 Frankfurt am Main, Germany
[3]ICAR3R-Interdisciplinary Centre for 3Rs in Animal Research, Faculty of Medicine, Justus Liebig University, 35390 Giessen, Germany
[4]Lead contact
*Correspondence: joe.howard@yale.edu
https://doi.org/10.1016/j.celrep.2023.113268

SUMMARY

Branching allows neurons to make synaptic contacts with large numbers of other neurons, facilitating the high connectivity of nervous systems. Neuronal arbors have geometric properties such as branch lengths and diameters that are optimal in that they maximize signaling speeds while minimizing construction costs. In this work, we asked whether neuronal arbors have topological properties that may also optimize their growth or function. We discovered that for a wide range of invertebrate and vertebrate neurons the distributions of their subtree sizes follow power laws, implying that they are scale invariant. The power-law exponent distinguishes different neuronal cell types. Postsynaptic spines and branchlets perturb scale invariance. Through simulations, we show that the subtree-size distribution depends on the symmetry of the branching rules governing arbor growth and that optimal morphologies are scale invariant. Thus, the subtree-size distribution is a topological property that recapitulates the functional morphology of dendrites.

INTRODUCTION

Branched morphologies are fascinating because they are ubiquitous in the natural world and often have high complexity.[1–4] In the case of neurons, the morphology of dendritic trees is functionally important because it defines where the cell can receive synaptic inputs from other neurons and how these inputs are integrated to allow signal transmission and computation.[5] The morphologies of dendrites are shaped during development by many cellular and molecular mechanisms including branching, elongation and retraction,[6,7] self-avoidance,[8] and morphogen gradients.[9] The resulting geometries, and in particular the lengths and spatial arrangements of the individual branches, often optimize electrical signaling by minimizing propagation times between sites of input and output.[10–17] Intracellular transport within branches delivers materials and nutrients to support the growth and activity of the cell.[18] Branch diameters, another important geometric property of neurons, may optimize the distribution of materials for growth and homeostasis[19–21] and the transfer of electrical currents.[17] Thus, the geometry of dendritic arbors—the lengths and diameters of their neurites—is functionally important because it constrains the transport of signals and materials within the cell. In this paper we asked whether the topology of dendritic arbors, those network properties that are invariant under deformations (homeomorphisms) of the arbor's geometry, is also important for neuronal function or growth.

The great diversity of the branching patterns of neurons[22] has spurred efforts to use topological concepts, in addition to geometry, to categorize neuronal morphologies into smaller numbers of distinct classes.[22–25] One avenue is topological data analysis (TDA), an approach to the analysis of data using techniques from topology to obtain information that is independent of the particular metrics[26]; this approach can reveal a system's intrinsic structure and distinguish that structure from other structures and noise.[27–29] The topological morphology descriptor (TMD), based on TDA, encodes the spatial structure of branched trees as a "barcode" and has been found to be useful for categorizing neurons.[30] In addition to TMD, which includes geometric information, there are several other topological measures that have been used to characterize the branching morphology of neurons. These include tree asymmetry,[31,32] Strahler ordering,[33–35] and subtree persistence.[36] Because the genetic networks responsible for pattern formation are frequently conserved through evolution, organisms of different size often have neuronal structures that scale geometrically.[37] Even for individual neurons, one might anticipate that repetitive application of a single set of pattern-formation rules[6,7,38] could generate arbors with similar geometric properties at different length scales, such as the fractal dimension.[39,40] Are there analogous topological properties that scale, and are these features functionally important?

In this study, we analyzed invertebrate[41,42] and vertebrate (NeuroMorpho.Org)[43] neurons and discovered a topological property of dendrites, the subtree-size distribution, that is often scale invariant. To appreciate the notion of topological scale invariance, we need some definitions. Each node or branchpoint in a tree defines a subtree comprising the set of branches that are distal to the node. We define the size of the subtree as the number of terminal branches, or tips, that the subtree supports.

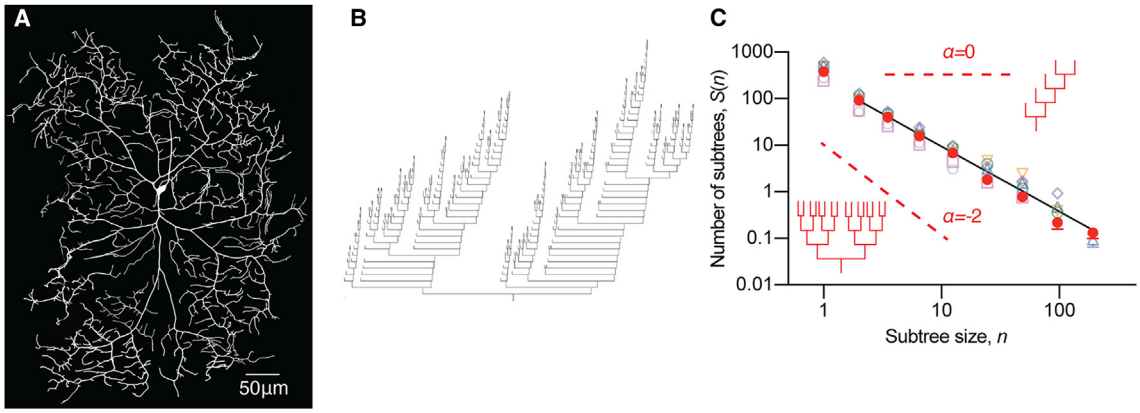

Figure 1. Subtree-size distributions for class IV sensory neurons follow a power law

(A) Dendritic arbor of a 96-h class IV neuron visualized with a GFP-tagged membrane marker by spinning-disk confocal microscopy (see STAR Methods).

(B) Dendrogram of the upper half of the arbor in (A).

(C) Subtree-size distribution for seven different dorsal class IV neurons from larval segments A3 to A5. The subtree size equals the number of tips. The solid symbols correspond to the cell in (A) and (B). The solid black line is the reduced major axis (RMA; see STAR Methods) fit to all the log-log data: the slope is -1.40 ± 0.04 (error stands for standard deviation from the RMA fitting). This corresponds to a perfection index of 0.70. The insets show a perfect tree (lower left) and a maximally imperfect tree (upper right) with slopes -2 and 0, respectively.

Because the number of tips is one more than the number of internal branches (those segments between two branchpoints), tip number is approximately one-half the total branch number and so serves as a proxy for subtree size. We found that for many neurons, the distribution of subtree sizes follows a power law, meaning that the distribution is linear when plotted on a log-log axis. This implies that the subtree-size distribution is scale invariant in the following sense: the distribution of subtrees of size cn (where c a constant) is proportional to the distribution of subtrees of size n (Newman et al., 2005[44] and STAR Methods, where we show that scale invariance is equivalent to a power law). Because different classes of neurons have different exponents in the power law (the slopes of the log-log plots), scale invariance can be used to distinguish cell types based on their topology. Through simulation, we show that scale invariance arises from iterative growth processes such as the Galton-Watson (GW) process.[45,46] The exponent depends on the bifurcation probability, the probability that a given dendritic tip will branch rather than terminate, as well as on the relative frequency of branching on internal, non-terminal branches. Furthermore, the presence of postsynaptic spines on mammalian neurons and of branchlets on *Drosophila* class III dendritic arborization (da) sensory neurons leads to characteristic deviations from a power law, suggesting that the spines and branchlets arise through different growth mechanisms compared to the proximal branches. Thus, the subtree-size distribution is a topological property that reflects the underlying branching morphogenesis of dendritic arbors and distinguishes the morphologies of different neuronal types.

RESULTS

Subtree-size distribution and perfection index

In our quest to uncover the underlying growth mechanisms of neurons, we investigated the topological properties of the dendritic arbors of class IV da cells in *Drosophila melanogaster* larvae (Figures 1A and 1B). These nociceptive cells form a dense meshwork of dendrites just under the cuticle; they detect attacks by the syringe-like ovipositor barbs of parasitic wasps and trigger escape responses.[47] With dendritic arbors having up to 2,000 branches and 1,000 tips (i.e., terminal branches) by the end of larval development (5–6 days after egg lay), class IV cells constitute a model system for studying dendrite morphogenesis.[41]

For a branched tree, such as a dendritic arbor, we define the subtree-size distribution[36,48] as the average number, S, of branches that support n dendrite tips (or leaves of the tree). The subtree-size distribution is a topological function that depends on the branching pattern of the dendrite. This is illustrated by the trees in the insets of Figure 1C. In a perfect, binary tree (lower left) each tip bifurcates at each branch order. The perfect tree shown has branch order (or height) 4 and has $2^4 = 16$ tips. The number of branches that support 16 tips is 1, the number that supports 8 tips is 2, and so forth. Because many tip numbers have no associated branches (e.g., in this example the number of branches that support three tips is zero), we bin and average. Specifically, we take geometrically increasing intervals of branch number: [0.5,1.5], [1.5,2.5], [2.5,4.5], [4.5,8.5], [8.5,16.5], and average the number of tips in each interval: $S(1) = 16$, $S(2) = 8, S(3.5) = 2, S(6.5) = 0.5, S(12.5) = 0.125$ (see Figure 1 legend). $S(1)$ equals the total number of tips. In this way, subtree-size distributions are calculated for single arbors. Note that the average number, S, can be less than 1 due to the normalization by interval size. For a perfect binary tree, the average decreases geometrically with a slope of approximately -2 when plotted using log-log axes (dashed red line on left). For the maximally imperfect tree (Figure 1C, upper right), each bifurcation leads to one terminal tip. In this case, the subtree-size density is $S(1) = 16, S(2) = 1, S(3.5) = 1, S(6.5) = 1, S(12.5) = 1$, which has slope zero on a log-log plot (dashed red line on right, omitting the first point).

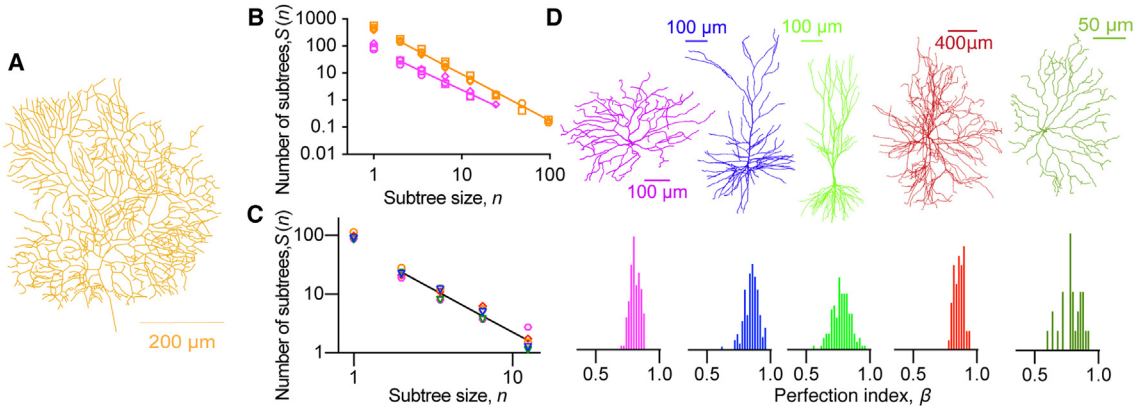

Figure 2. Dendrite subtree-size distributions and perfection indices for neurons in the central nervous systems of vertebrates and invertebrates

(A) Skeletonized guinea pig cerebellar Purkinje cell[49] in which branches have been replaced by their center lines.

(B) Subtree-size distributions for four Purkinje cells (orange) and three retinal ganglion cells (magenta): the perfection indices are 0.86 ± 0.02 and 0.76 ± 0.04, respectively.

(C) Subtree-size distributions for the five *Drosophila* T5 cells shown in Figure S3. The perfection index is 0.73 ± 0.04. We did not include error bars in (B) and (C) because they are small.

(D) Perfection indices measured from reconstructed neurons from the morphological database www.neuromorpho.org. Retinal ganglion cells: 0.80 ± 0.04 (magenta, n = 130 cells); neocortical pyramidal cells: 0.85 ± 0.06 (blue, n = 165 cells); hippocampal pyramidal cells: 0.78 ± 0.07 (green, n = 131 cells); motoneurons: 0.86 ± 0.04 (red, n = 56 cells); starburst amacrine cells: 0.79 ± 0.08 (dark green, n = 27 cells). All errors are standard deviations.

Based on these empirical properties, if $S(n)$ scales linearly with tip number n (on a log-log plot), with power-law exponent $-\alpha$, we define the perfection index $\beta = \alpha/2$ (Figure S1). The intuition behind the perfection index is that a "perfect" binary tree, which is defined as one in which every tip bifurcates at each order, has a perfection index $\beta = 1$ (oblique red dashed line in Figure 1C). A perfection index, $\beta = 0$, corresponds to a "maximally imperfect" tree in which one tip bifurcates and the other terminates (horizontal red dashed line in Figure 1C).

The subtree-size distribution follows a power law for class IV neurons

The subtree-size distributions for the dendritic arbors of class IV cells follow a power law: they are straight lines when plotted against tip number on a log-log axis (Figure 1C). Thus, we can write $S(n) = n_{\text{total}} n^{-\alpha}$ for n between 1 and n_{total}. The average value of the exponent is $\alpha = 1.40$ with corresponding perfection index of 0.70. Thus, class IV cells are imperfect binary trees with slopes lying between the extremes of perfect and maximally imperfect.

The subtree-size distribution follows a power law for a wide variety of neurons

To test whether the perfection-index concept can be generalized to neurons from other species, we analyzed guinea pig Purkinje cells (Figure 2A).[49–51] Figure 2B shows that the power law holds with an exponent of 1.72 and corresponding perfection index of 0.86. The plot of normalized residuals for class IV and Purkinje cells confirmed the goodness of fit (Figure S2). Mouse retinal ganglion cells[52] also satisfied a power law, with a perfection index of 0.76 (Figure 2B).

Next, we asked whether the power law generalizes to the central nervous system of adult flies. We analyzed *Drosophila* T5 cells, which are in the motion-sensing pathway (Figure S3, from Scheffer et al.[42]). T5 cells remain relatively stable in size during adulthood, in contrast to class IV cells, which grow continuously through larval development.[7] As shown in Figure 2C, the power law holds with an average perfection index of 0.75.

We further analyzed the dendritic trees of different cell types from the NeuroMorpho database[43] including: Purkinje cells from the cerebellums of guinea pig, rat, and mouse; spinal motoneurons from rat and cat; retinal ganglion cells from mouse, pouched lamprey, and salamander; pyramidal cells in the hippocampus of rat, mouse, and guinea pig; pyramidal neurons in the neocortical layers of rat, mouse, cat, monkey, and human; and starburst amacrine cells from monkey, mouse, and rabbit. The power law holds for these neurons, with mean perfection indices ranging from 0.78 to 0.86 (Figure 2D). While the total range of indices is small, 0.70 (*Drosophila* class IV neurons) to 0.86 (cerebellar Purkinje cells), the means differ significantly between different cell types because the standard errors are small (<0.01). Thus, the perfection index is a metric that distinguishes different classes of neurons.

Perfection index is unchanged under trimming and ablation

When we iteratively trimmed the terminal branches of class IV neurons, the subtree-size distribution still followed a power law, with a perfection index similar to that of the original neuronal tree (Figures 3A–3D). Trimmed Purkinje cells also followed a power law, although the exponents decreased (Figure 3E). When we randomly ablated internal branches of class IV neurons (Figures 3F and 3G), the subtree-size distributions continued to follow power laws (Figure 3H). The perfection indices of both class IV and Purkinje cells were similar after ablation (Figure 3I). Thus, the subtree-size distributions are self-similar under these perturbations, with similar perfection indices.

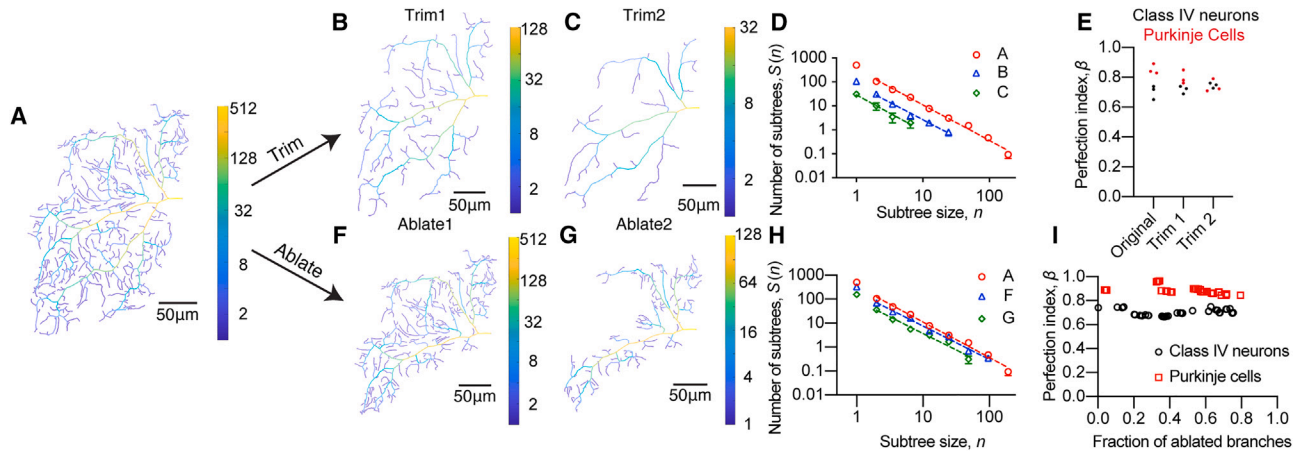

Figure 3. The perfection index is invariant under branch trimming and ablation

(A–D) (A) Part of a class IV arbor with supported tips colored according to the scale at right. (B) Arbor A after trimming (i.e., removing terminal branches). (C) Arbor A after trimming a second time. (D) The perfection indices are 0.74 (A), 0.73 (B), and 0.76 (C).

(E) Perfection indices of class IV and Purkinje cells before and after trimming.

(F) Arbor A after randomly ablating 35% of branches.

(G) Arbor A after randomly ablating 69% of branches.

(H) The perfection indices are 0.74 (A), 0.70 (F), and 0.69 (G).

(I) Perfection indices from class IV neurons and Purkinje cells following branch ablation.

Percolation transition associated with the Galton-Watson branching process

To gain insight into why neurons have subtree-size distributions that can be described by a power law with a narrow range of exponents, we initially studied one of the simplest models for generating trees, the GW process.[45] In a binary GW process,[46] each terminal branch (denoted by B) bifurcates into two new terminal branches with probability p, or stops bifurcating to form a tip (denoted by T) with probability $1 - p$:

$$\mathrm{B} \rightarrow \begin{cases} \mathrm{B} & \mathrm{Prob} = p \\ \mathrm{T} & \mathrm{Prob} = 1 - p \end{cases} \qquad \text{(Equation 1)}$$

When $p = 1$, the GW process produces a perfect tree, which is deterministic in the sense that every tree is identical. When $p < 1$, the GW process produces an imperfect tree, with an arborization pattern that varies from tree to tree, even for the same value of p.

The GW process (illustrated in Figure 4A) produces random binary trees (gray lines in Figure 4A) that are a subset of a perfect tree (black lines in Figure 4A). If the bifurcation probability p is >0.5, then on average at least one of the terminal branches will continue to bifurcate. The number of branches is expected to increase with branch order. Otherwise, when $p < 0.5$, the average number of branches will decrease with the branch order, and growth will almost surely terminate. The critical bifurcation probability, $p_c = 0.5$, therefore marks a qualitative change in the behavior of a binary branching process, with supercritical ($p > 0.5$) trees able to reach high branch orders. This behavior is analogous to a percolation transition, which describes the emergence of long-range connectivity in random systems when a critical value, known as the percolation threshold, is exceeded.[53]

Stochastic simulations showed that the GW process (with $p > 0.5$) produces trees whose subtree-size distributions follow power laws (Figure S4A). The perfection index increased from 0.7 to 1 as p increased from 0.5 to 1 (Figure 4B, black squares). Interestingly, bifurcation probabilities larger than the percolation threshold $p_c = 0.5$ and smaller than 0.7 (Figure 4B, red region) correspond to the perfection indices observed over a wide variety of neurons (0.70–0.86).

GW processes with variable bifurcation probabilities also show power-law behavior

We next asked whether more general growth processes also lead to subtree-size distributions that follow power laws. In a generalized GW process the bifurcation probability, $p(d)$, depends on the branch order, d.[45] For any tree, we can also measure the probability, $P(d)$, that branches of order d bifurcate; Figure 5A shows $P(d)$ measured for a class IV cell. Note that the measured P for a simulated tree does not necessarily equal p because growth is stochastic; indeed, growth fluctuations may cause any simulated tree with $p < 1$ to terminate eventually, even when $p > 0.5$ for all d (i.e., $P(d) = 0$ for d sufficiently large). For a finite tree, the measured bifurcation probability P must fall below 0.5 at high branch order. For simulated trees, termination can happen in a number of ways: there might be an abrupt decrease in p to zero at some branch order, or p might decrease to a value close to or below the critical value of $p_c = 0.5$, so that the tree slowly stops growing as found in class IV neurons (Figure 5A). We performed simulations using the two branch-order-dependent bifurcation probabilities shown in Figure 5B. In both cases, the subtree-size distribution $S(n)$ vs. n follows a power law as shown in Figure 5C. Binary trees grown with higher bifurcation probabilities at lower branch order have higher

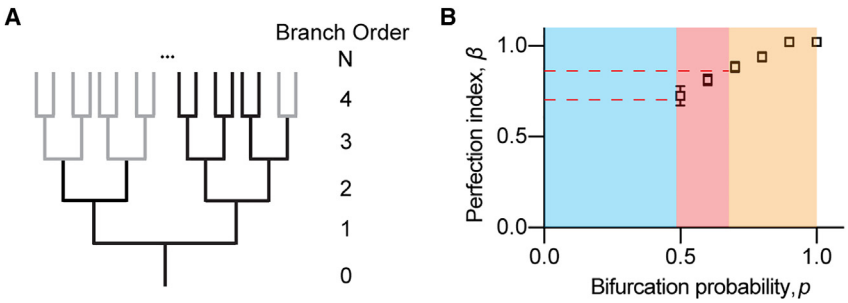

Figure 4. Percolation transition associated with the Galton-Watson branching process

(A) An example binary tree (black lines) superimposed on a perfect binary tree (light-gray lines) with order 4.

(B) Perfection index β as a function of branching probability p. For each branching probability, trees with total tip number of approximately 400 were analyzed with 100 simulations for each bifurcation probability. The blue-shaded region corresponds to the region below the percolation transition. The red-shaded region corresponds to the perfection-index range observed in this work. The orange-shaded region is outside the observed range. Error bars are SDs.

perfection indices (Figure 5B vs. Figure 5C). This observation is consistent with the simulation results (Figure 4B), where higher bifurcation probability leads to higher perfection indices.

Next, we asked whether the correlation between bifurcation probabilities and perfection indices also applies to real dendrites. The measured perfection index for Purkinje cells (0.86, Figure 2B) is larger than that for class IV neurons (0.70, Figure 1C). Notably, Purkinje cells have a higher bifurcation probability, P, than class IV cells at lower branch orders, but lower probability at higher orders (Figure 5A vs. Figure 5D). The higher perfection indices of Purkinje cells compared to class IV cells indicate that the bifurcation probability during the early stages of growth may be an important determinant of the perfection index. Moreover, simulations performed with measured bifurcation probabilities vs. branch order (Figures 5A and 5D, see STAR Methods) as input were able to reproduce the experimentally observed perfection indices (Figure S4B). Thus, the subtree-size distribution of class IV and Purkinje cells are consistent with GW processes with order-dependent bifurcation probabilities.

Quantifying the degree to which dendritic morphologies are stochastic vs. deterministic

The correlation between the bifurcation probability in the GW process and the perfection index allows us to relate the stochasticity of a tree to its perfection index. If the branches with a given order bifurcate with probability p, the mean number of new branches at the next higher order is proportional to $2p$ and the variance is proportional to $4p(1-p)$. Therefore, the variance in the number of new branches is greatest when $p = 0.5$, the percolation threshold, and decreases to zero as p increases to 1. Hence, we can say that for $p > 0.5$, a smaller bifurcation probability (lower perfection index) is more stochastic whereas a larger bifurcation probability (higher perfection index) is more deterministic. By this measure, the growth rules for mammalian Purkinje cells are more deterministic and less stochastic than insect class IV neurons.

Density constraints account for why the bifurcation probability is close to 0.5

We asked why the measured bifurcation probabilities are approximately 0.5 for many branch orders (Figures 5A and 5D). One possible explanation is that arbor volume constrains bifurcation. It is clear when considering a perfect tree that the only way to fit in the highest-order branches is to decrease the spacing between branches. If the area per branch (in 2D) or the volume per branch (in 3D) remains constant during growth, however, then p must decrease. This can be seen by considering a circular arbor with constant dendrite density. The number of highest-order branches is proportional to the perimeter, which in turn is proportional to the radius, which is proportional to the branch order, d (by the constant density assumption). If all the peripheral tips were to bifurcate, the number of new branches in the next growth ring would be proportional to $2d$; but the outer perimeter of the growth ring can only support a number of branches proportional to the new perimeter $(d+1)$. Thus, we expect $p_{2D} \rightarrow (d+1)/2d = 1/2 + 1/2d$. In 3D, $p_{3D} \rightarrow (d+1)^2/2d^2 = 1/2 + 1/d$. This shows that a constant branch density constrains the bifurcation probability to approach 0.5, the percolation threshold, as observed.

Internal vs. tip branching

Class IV cells grow by a stochastic branching process in which new branches can form either on terminal dendrites, which we call tip branching and is topologically equivalent to tip bifurcation, or on internal (non-terminal) branches.[7] The frequency of internal and tip branching is approximately equal. By contrast, Purkinje cells in culture grow predominantly by tip branching.[6] We therefore analyzed so-called QS growth processes[32] that have a balance between internal and tip branching (here we considered the one-parameter model[54]; Figure S6). We found that internal branching, provided its frequency is less than tip branching, still gives rise to a power law, and that the perfection index decreases as the relative frequency of internal branching increases (Figure S6B). Deviations from a power law occur when the frequency of internal branching exceeds that of tip branching (Figure S6C). Thus, more general branching mechanisms that include internal branching also give rise to power laws, at least over a range of internal branching frequencies, although the exponents are lower.

Neuronal branching patterns that optimize wiring also follow a power law

In addition to the GW and QS processes, we also tested whether other morphogenetic processes give rise to power laws for their subtree-size distributions. Cuntz et al.[13,55] proposed a method of constructing branched networks based on an optimal wiring principle. To connect a given distribution of synapses or a sites of sensory reception to a single point, the cell body, they

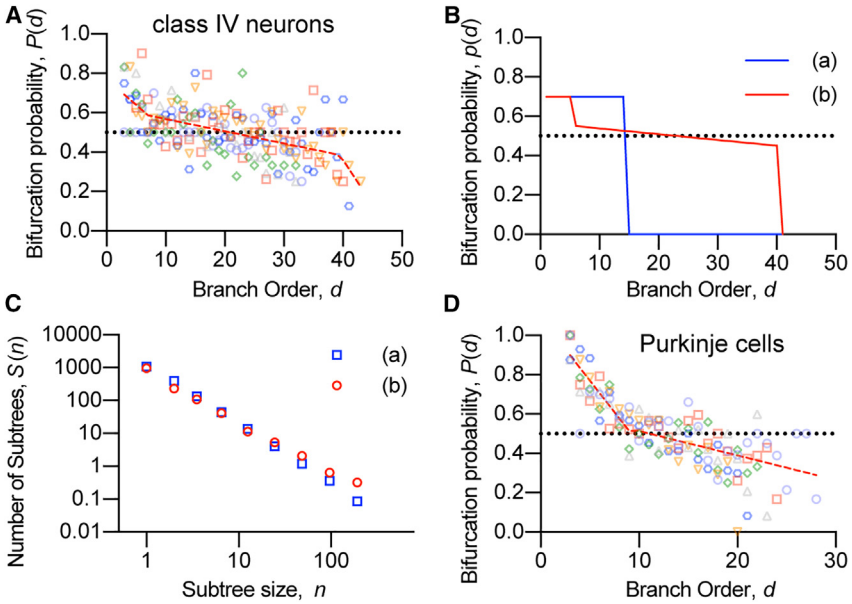

Figure 5. The power-law exponent varies with the order-dependence of the bifurcation probability in the Galton-Watson process

(A) Bifurcation probabilities as a function of branch order for class IV neurons.

(B) Two bifurcation probability functions. The blue curve shows an abrupt decrease of bifurcation probability from 0.7 to 0 at branch order 15. The red dashed curve shows a decrease from 0.7 to 0.55 at branch order 6 and a gradual change from 0.55 to 0.45 from branch order 7 to branch order 40, followed by an abrupt change to 0.

(C) $S(n)$ vs. n for the two cases in (B) follow power laws, although the slopes differ. The exponent in (a) is $\alpha = 1.79$ and in (b) is $\alpha = 1.52$.

(D) Bifurcation probabilities as a function of branch order for Purkinje cells.

In (A) and (D), six neurons were analyzed with different colors representing different animals. The bifurcation probability was only calculated for orders with six or more branches. The black dotted line shows a bifurcation probability of 0.5. A linear piecewise fit (dashed red lines) is overlaid.

extended the concept of a minimum spanning tree to construct trees that weigh the costs of material (total dendrite length) against the conduction time (path length to soma) using a single regularization parameter, the balancing factor, *bf*. The balancing factor (BF) has proved to be an effective method to describe a wide variety of neuronal structures from insect dendrites to mammalian neurons.[13,56] A smaller balancing factor, *bf*, leads to a more branched structure, in which the neuron utilizes its limited cytoskeletal resources more efficiently to fill up a large space. A larger balancing factor results in fewer bifurcations and more direct connections to the soma so that conduction times are reduced.

To test whether trees generated by the balancing-factor (BF) process display power laws, we randomly distributed points to mimic synaptic sites and created optimal-wired synthetic trees starting at the center point according to the balancing factor from 0 to 1 in steps of 0.1 (Figure 6A). The subtree-size distribution followed a power law with the perfection index increasing monotonically from 0.67 to 0.81 as *bf* increased from 0 to 0.9 (Figure 6B); this falls within the experimentally measured range of perfection indices. Moreover, this finding is consistent with the conclusions from previous studies that balancing factors in the range of 0.0–0.9 can be used to describe a wide variety of neurons in *Drosophila* sensory neurons and hippocampal granule cells.[13,56]

Comparison between the perfection index and tree asymmetry

The perfection index is also related to another topological measure, tree asymmetry.[32] The asymmetry of a branch whose daughters support l and m tips ($l \leq m$) is defined as $(m - l)/(l + m - 2)$; if l=m the asymmetry is zero and if $l = 1$ the asymmetry is 1. The asymmetry of the tree is the weighted average of the branch asymmetry.[32] We compared the perfection index and the tree asymmetry for neurons from the NeuroMorpho and Hemibrain datasets (density plot as shown in Figure 6C) and found that the data cluster around perfection indices of 0.8 and asymmetry 0.5. When we generated trees using the GW process with different values of p and measured both the perfection index and tree asymmetry, we found that they are inversely correlated, as shown by the gray dotted curve in Figure 6C, which passes through the experimental data. This is consistent with our earlier observation that a higher perfection index is associated with higher symmetry of the arbors. In earlier studies, tree asymmetry was also found to be invariant under trimming (terminal pruning) and ablation (random pruning),[57] further highlighting the close relationship between these two topological measures. Because tree asymmetry has a larger coefficient of variation compared with the perfection index, it might better distinguish the morphologies of different neuronal types.

Two-step growth mechanisms lead to deviations of the subtree-size distribution from a power law

Next, we asked whether every morphogenetic process gives rise to power-law behavior of the subtree-size distribution. The answer is no.

There are four classes of sensory neurons that tile the larval body wall of flies.[58] The morphology of class III neurons differs from that of class IV neurons in having short terminal branchlets along most of their lengths (Figure 7A). The subtree-size distribution of class III cells shows two phases (Figure 7B): a shallower slope for small tip numbers (exponent of 0.84) and a steeper slope for larger tip numbers (exponent of 1.52). When we removed all the branchlets from a class III neuron, leaving only the backbone (Figure S5), we found that the subtree-size distribution followed a power law (Figure 7C) similar to that of class IV neurons with an exponent of 1.50. When we added back branchlets at random locations along the backbone, we recovered the two-phase behavior of the subtree-size distribution (Figure 7B). Thus, class III cells have a backbone with a

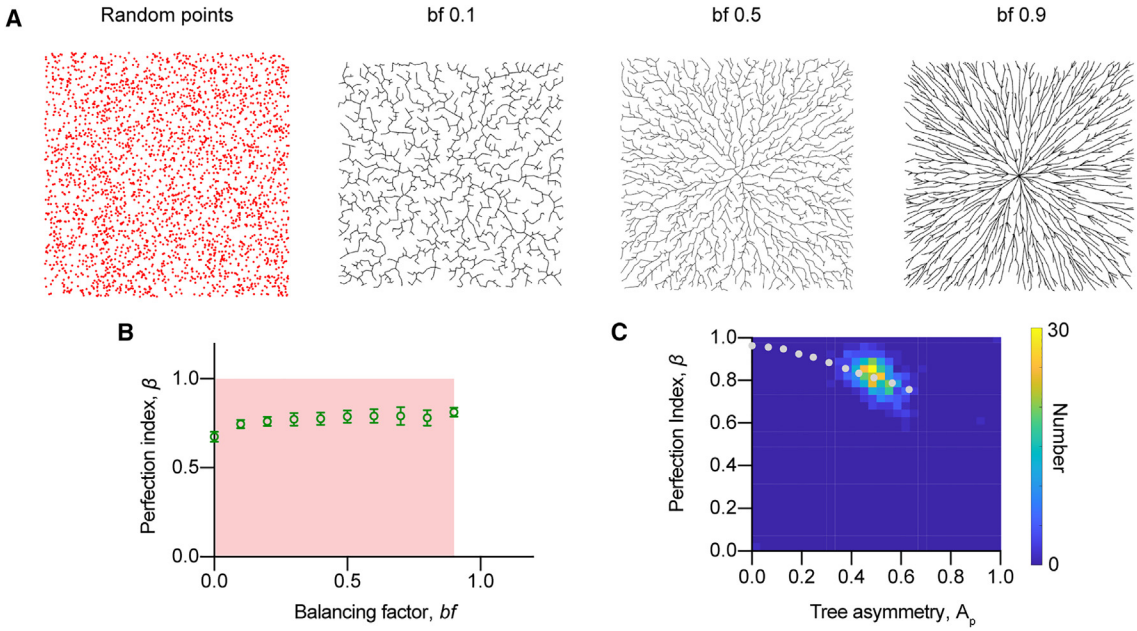

Figure 6. Perfection indices of trees generated by the optimal wiring and with different asymmetries

(A) Example trees grown from randomly distributed points (left panel) from a root at the center. As the balancing factor (*bf*) increases, the branches become more radial as the trade-off shifts from smaller total branch length to shorter path distances to the center (see text).

(B) Perfection index β is plotted as a function of balancing factor. The red shadowed region indicates the region that falls within the experimentally observed range (determined by [mean − 2SD, mean + 2SD]). Each data point is averaged from 100 simulations. Error bars are standard deviations.

(C) A comparison between the tree asymmetry, A_p, and the perfection index, β, measured for 532 cells from NeuroMorpho and Hemibrain databases. $A_p = 0.50 \pm 0.07$ and $\beta = 0.82 \pm 0.07$ (mean ± SD, n = 532). The dotted curve is obtained from the GW model.

perfection index similar to that of class IV cells, with the difference in the subtree-size distribution arising from terminal branchlets. This observation suggests that primary branches of class III cells grow by a developmental mechanism similar to that of class IV cells, i.e., with bifurcation probability above the percolation threshold, followed by the random addition of branchlets, consistent with a recent paper demonstrating that a two-step model is necessary to describe the class III neuron morphology.[59]

Like class III neurons, the subtree-size distributions of pyramidal cells with spines from layer 2/3 of the mouse cortex (Figure 7D, MICrONs datasets, see STAR Methods) also deviate from power laws as shown in Figure 7E. The subtree-size distribution showed two phases, a shallow slope (exponent 0.08) and a steeper slope with (exponent 1.77). When we removed all spines and measured the subtree-size distribution, a power law was recovered with an average exponent of 1.6 (Figure 7F). Note that the pyramidal and Purkinje cells analyzed in Figure 2 did not include spines. Again, adding artificial spines through simulations recovers the experimental observation as shown in Figure 7E. It is noteworthy that although the power-law behavior can be disrupted when internal branching exceeds tip bifurcation, the two-phase behavior cannot be achieved by the QS process alone (when *S* is kept at zero, i.e., one-parameter model, Figure S6C). This further suggests that a two-step model is necessary. Thus, subtree-size distributions can deviate from a power law and exhibit two-phase behaviors, indicating distinctive growth mechanisms.

DISCUSSION

In this study, we found that the subtree-size distribution, which is a purely topological property of branched networks, follows a power law for many, but not all, neurons. When the distribution follows a power law, we can define the perfection index as half of the power-law exponent; a value of 1 corresponds to a perfect binary tree in which the number of branches doubles at each order, and a value less than 1 corresponds to an imperfect tree in which branching is stochastic and eventually terminates. By analyzing neurons from the NeuroMorpho.Org and Hemibrain datasets, we found that the perfection index falls within the range 0.70–0.86 for a wide range of vertebrate and invertebrate neurons and that the value of the perfection index distinguishes different neuronal types: for example, mammalian Purkinje cells have a perfection index of 0.86 while fly class IV da neurons have a perfection index of 0.70. Moreover, these values are often invariant to iterative trimming of terminal branches and ablation of internal branches, suggesting that in these cells the branching rules may persist as the neuron grows and that the subtree structures are self-similar. We found exceptions to power laws when spines and branchlets were included in the analysis, consistent with these terminal branches arising through growth processes that differ from those of the backbone arbor. Thus, the subtree-size distribution is a topological property that reflects the functional morphology of dendrites and, as discussed below, likely recapitulates the morphogenetic processes, i.e., the ontogeny, underlying branching.

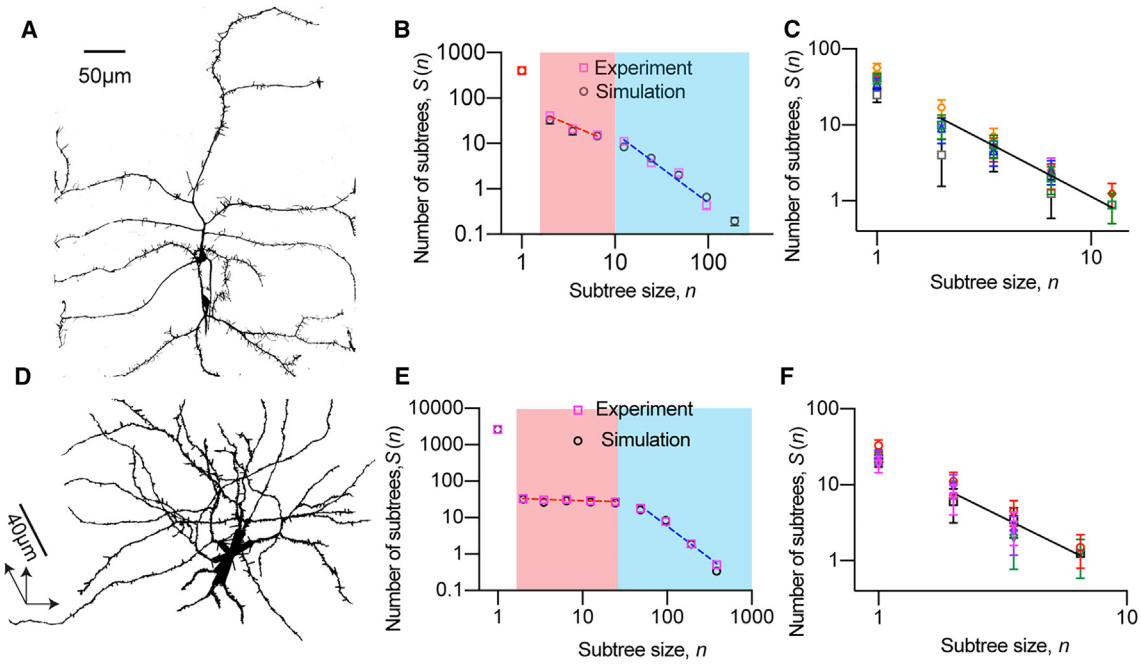

Figure 7. Spines and branchlets lead to deviations from a power law

(A) A GFP-labeled 96-h class III dorsal neuron in the A4 segment imaged by spinning-disk confocal microscopy. It has short branchlets along its branches.

(B) The "two-phase" behavior of the subtree-size distribution. The red and blue regions have different slopes (represented by dashed lines).

(C) Subtree-size distributions for backbones of six different class III neurons (with terminal branches trimmed) in the A3 to A5 segments from both dorsal and ventral sides fit a power law with exponent 1.47 (perfection index 0.74). Error bars are SDs.

(D) A pyramidal cell from layer 2/3 of mouse visual cortex segmented from the MICrONS electron microscopy dataset. It has spines along its length.

(E) Two-phase behavior of the pyramidal cell with spines is observed.

(F) The subtree-size distribution of six trimmed pyramidal cells has a power-law exponent 1.61 (perfection index 0.81). Error bars are SDs.

To gain a theoretical understanding of the subtree-size distribution and why it follows a power law, we compared the neuronal data to the predictions of several mathematical morphogenetic processes, including the GW process in which tips bifurcate, the QS process,[32,60] which has both tip bifurcation (tip branching) and internal (non-tip) branching, and the optimal-wiring BF process,[13,55] which trades off total branch length against distance to the cell body. All produce subtree-size distributions that follow power laws and so are consistent with the observed topologies. In the GW process, the power-law exponent increases with the bifurcation probability, while in the QS process, the exponent decreases with increasing internal branching (relative to tip branching). It is likely that the higher exponent in Purkinje cells than in class IV arises from both effects. First, at low branch orders, the measured bifurcation probability of Purkinje cells is higher than that of class IV cells (Figure 5D vs. Figure 5A); this is expected to lead to a higher perfection index. Second, cultured Purkinje cells make fewer internal branches than tip branches (90% of new branches occur on terminal branches[6] and only 10% on internal branches), while class IV cells *in vivo* make similar numbers of terminal and non-terminal branches[7]; this difference is also expected to increase the perfection index of Purkinje cells relative to class IV cells. These two effects are not mutually exclusive. An increase in tip branching relative to internal branching results in higher branching probabilities at low branch orders (Figures S6D and S6E). Thus, it is likely that multiple developmental differences give rise to the different topologies of class IV and Purkinje cells.

Power laws in physics are often associated with phase transitions.[61] A phase transition that may be pertinent to dendrite branching is percolation: the GW process has a percolation threshold when the bifurcation probability is 0.5. Above 0.5, the number of branches increases, on average, at each order and below 0.5 it decreases. Any observed finite tree must have a measured bifurcation probability that decreases below 0.5 at high orders. Furthermore, as we argued in the results section, if there is a minimum branch density, space constraints cause the GW bifurcation probability to approach 0.5. Therefore, there are theoretical reasons why dendritic trees should have bifurcation probabilities near 0.5, at least at high orders. Consistent with this argument, measured bifurcation probabilities of both class IV cells and Purkinje cells both have wide ranges of orders where $P \cong 0.5$. Thus, the growth of dendritic arbors is close to a percolation threshold, and this may contribute to the power-law behavior.

Time-lapse imaging of dendrites *in vivo* (e.g., class IV cells[7]) and *in vitro* (e.g., Purkinje cells[6]) shows that morphogenesis often entails iteration of growth rules that remain fairly constant over time. Two features of the subtree-size distribution likely reflect this iterative process. First, the observation that the subtree-size distribution is scale invariant (i.e., follows a power law) for many cell types suggests the branching process is invariant/self-similar over

development. Second, the observation that trimming and ablating arbors preserves the power law and its exponent suggests that later growth occurs by the same rules as earlier growth. In the cases of class III neurons and mammalian neurons, branchlets and spines perturb the subtree-size distribution from a power law, consistent with an altered growth process during development. Interestingly, in branchlets[59] and spines,[62] actin plays a prominent role, while in of the dendritic shaft or "backbone," microtubules are prominent structures that serve as tracks for long-distance transport.[63] Thus, branchlets and spines use different cytoskeletal machineries compared to the backbone, and this may disrupt the iterative growth process and perturb the subtree-size distribution.

In summary, the subtree-size distribution provides a simple quantitative description of the topology of neuronal morphologies. While it lacks the richness of other schemes for classifying neuronal morphology, such as the TMD,[30] the power-law exponent can still distinguish different cell types and different growth rules. The subtree-size distribution simplifies study of the structure of neurons and thus provides an important additional constraint that must be fulfilled by other methods for generating dendritic trees.

Limitations of the study

Despite its success in identifying a consistent signature of dendritic structure and evidence for distinct growth processes, our study has several limitations. First, accurately measuring the subtree-size function requires a large number of branches, on the order of 100, limiting its utility to highly branched cells. For smaller trees other measures like asymmetry[32] should be used. Second, subtree-size distributions are not generative, in the sense that they can be used to grow arbors; indeed, different growth processes with different bifurcation probabilities and internal-to-tip branching ratios can generate similar subtree-size distributions. Third, as more neurons are added to the rapidly expanding morphological databases, exceptions to our findings are likely to increase. Finally, theoretical studies are needed to establish rigorously whether there exist conditions necessary and sufficient for scale invariance of subtree-size distributions.

STAR★METHODS

Detailed methods are provided in the online version of this paper and include the following:

- KEY RESOURCES TABLE
- RESOURCE AVAILABILITY
  - Lead contact
  - Materials availability
  - Data and code availability
- EXPERIMENTAL MODEL AND SUBJECT DETAILS
  - Drosophila melanogaster strains
- METHOD DETAILS
  - Scale invariance and power laws
  - Spinning disk confocal imaging
  - Data processing method
  - Reduced major axis (RMA) linear regression method
  - Perfection index calculation
  - Bifurcation probability measurement from experimentally reconstructed neurons
  - Methods for MICrONS dataset analysis
  - Simulating trees with balancing factors

SUPPLEMENTAL INFORMATION

Supplemental information can be found online at https://doi.org/10.1016/j.celrep.2023.113268.

ACKNOWLEDGMENTS

The authors thank Dr. Thomas Torng and Dr. Yin-Wei Kuo for their invaluable feedback on this work. This work was supported by NSF GR117147 (J.H.), NIH R01 NS118884 (J.H.), a Burroughs Wellcome Career Award at the Scientific Interface (M.L.), BMBF no. 031L0229 (A.D.B.), and Deutsche Forschungsgemeinschaft (DFG, German Research Foundation) no. 467764793, JE 528/10-1 (A.D.B.).

AUTHOR CONTRIBUTIONS

Conceptualization, M.L. and J.H.; methodology, M.L. and J.H.; software, A.D.B., M.L., and H.C.; validation, A.D.B. and H.C.; formal analysis, M.L., J.H., A.D.B., and H.C.; writing – review & editing, M.L., J.H., A.D.B., and H.C.; supervision, J.H.

DECLARATION OF INTERESTS

The authors declare no competing interests.

INCLUSION AND DIVERSITY

We support inclusive, diverse, and equitable conduct of research.

Received: February 27, 2023
Revised: August 1, 2023
Accepted: September 28, 2023

REFERENCES

1. Goodwin, K., and Nelson, C.M. (2020). Branching morphogenesis. Development *147*, dev184499. https://doi.org/10.1242/dev.184499.
2. Hannezo, E., and Simons, B.D. (2019). Multiscale dynamics of branching morphogenesis. Curr. Opin. Cell Biol. *60*, 99–105. https://doi.org/10.1016/j.ceb.2019.04.008.
3. Iber, D., and Menshykau, D. (2013). The control of branching morphogenesis. Open Biol. *3*, 130088. https://doi.org/10.1098/rsob.130088.
4. Ochoa-Espinosa, A., and Affolter, M. (2012). Branching morphogenesis: from cells to organs and back. Cold Spring Harb. Perspect. Biol. *4*, a008243. https://doi.org/10.1101/cshperspect.a008243.
5. Ramón y Cajal, S. (1911). Histology of the Nervous System of Man and Vertebrates.
6. Fujishima, K., Horie, R., Mochizuki, A., and Kengaku, M. (2012). Principles of branch dynamics governing shape characteristics of cerebellar Purkinje cell dendrites. Development *139*, 3442–3455. https://doi.org/10.1242/dev.081315.
7. Shree, S., Sutradhar, S., Trottier, O., Tu, Y., Liang, X., and Howard, J. (2022). Dynamic instability of dendrite tips generates the highly branched morphologies of sensory neurons. Sci. Adv. *8*, eabn0080. https://doi.org/10.1126/sciadv.abn0080.
8. Grueber, W.B., and Sagasti, A. (2010). Self-avoidance and tiling: mechanisms of dendrite and axon spacing. Csh Perspect Biol *2*, a001750. https://doi.org/10.1101/cshperspect.a001750.

9. Lin, T.-Y., Chen, P.-J., Yu, H.-H., Hsu, C.-P., and Lee, C.-H. (2020). Extrinsic factors regulating dendritic patterning. Front. Cell. Neurosci. *14*, 622808. https://doi.org/10.3389/fncel.2020.622808.

10. Wen, Q., and Chklovskii, D.B. (2008). A cost–benefit analysis of neuronal morphology. J. Neurophysiol. *99*, 2320–2328. https://doi.org/10.1152/jn.00280.2007.

11. Cuntz, H., Bird, A.D., Mittag, M., Beining, M., Schneider, M., Mediavilla, L., Hoffmann, F.Z., Deller, T., and Jedlicka, P. (2021). A general principle of dendritic constancy: A neuron's size- and shape-invariant excitability. Neuron *109*, 3647–3662.e7. https://doi.org/10.1016/j.neuron.2021.08.028.

12. Cuntz, H., Mathy, A., and Häusser, M. (2012). A scaling law derived from optimal dendritic wiring. Proc National Acad Sci *109*, 11014–11018. https://doi.org/10.1073/pnas.1200430109.

13. Cuntz, H., Forstner, F., Borst, A., and Häusser, M. (2010). One rule to grow them all: a general theory of neuronal branching and its practical application. PLoS Comput. Biol. *6*, e1000877. https://doi.org/10.1371/journal.pcbi.1000877.

14. Rall, W. (1964). In Theoretical Significance of Dendritic Trees for Neuronal Input-Output Relations, R.F. Reiss, ed. (Stanford Unv. Press).

15. Cuntz, H., Borst, A., and Segev, I. (2007). Optimization principles of dendritic structure. Theor. Biol. Med. Model. *4*, 21. https://doi.org/10.1186/1742-4682-4-21.

16. Jaffe, D.B., and Carnevale, N.T. (1999). Passive normalization of synaptic integration influenced by dendritic architecture. J. Neurophysiol. *82*, 3268–3285. https://doi.org/10.1152/jn.1999.82.6.3268.

17. Bird, A.D., and Cuntz, H. (2016). Optimal current transfer in dendrites. PLoS Comput. Biol. *12*, e1004897. https://doi.org/10.1371/journal.pcbi.1004897.

18. Sterling, P., and Laughlin, S. (2015). Principles of Neural Design (MIT Press).

19. Liao, M., Liang, X., and Howard, J. (2021). The narrowing of dendrite branches across nodes follows a well-defined scaling law. Proc National Acad Sci *118*, e2022395118. https://doi.org/10.1073/pnas.2022395118.

20. Donovan, E.J., Agrawal, A., Liberman, N., Kalai, J.I., Chua, N.J., Koslover, E.F., and Barnhart, E.L. (2022). Dendrite architecture determines mitochondrial distribution patterns in vivo. Preprint at bioRxiv, 2022.07.01.497972. https://doi.org/10.1101/2022.07.01.497972.

21. Williams, A.H., O'Donnell, C., Sejnowski, T.J., and O'Leary, T. (2016). Dendritic trafficking faces physiologically critical speed-precision tradeoffs. Elife *5*, e20556. https://doi.org/10.7554/elife.20556.

22. Markram, H., Toledo-Rodriguez, M., Wang, Y., Gupta, A., Silberberg, G., and Wu, C. (2004). Interneurons of the neocortical inhibitory system. Nat. Rev. Neurosci. *5*, 793–807. https://doi.org/10.1038/nrn1519.

23. Petilla Interneuron Nomenclature Group; Ascoli, G.A., Alonso-Nanclares, L., Anderson, S.A., Barrionuevo, G., Benavides-Piccione, R., Buzsáki, G., Buzsáki, G., Cauli, B., Fairén, A., et al. (2008). Petilla terminology: nomenclature of features of GABAergic interneurons of the cerebral cortex. Nat. Rev. Neurosci. *9*, 557–568. https://doi.org/10.1038/nrn2402.

24. DeFelipe, J., López-Cruz, P.L., Benavides-Piccione, R., Bielza, C., Larrañaga, P., Anderson, S., Burkhalter, A., Cauli, B., Fairén, A., Feldmeyer, D., et al. (2013). New insights into the classification and nomenclature of cortical GABAergic interneurons. Nat. Rev. Neurosci. *14*, 202–216. https://doi.org/10.1038/nrn3444.

25. Gouwens, N.W., Sorensen, S.A., Baftizadeh, F., Budzillo, A., Lee, B.R., Jarsky, T., Alfiler, L., Baker, K., Barkan, E., Berry, K., et al. (2020). Integrated morphoelectric and transcriptomic classification of cortical GABAergic cells. Cell *183*, 935–953.e19. https://doi.org/10.1016/j.cell.2020.09.057.

26. Carlsson, G. (2009). Topology and data. B Am Math Soc *46*, 255–308. https://doi.org/10.1090/s0273-0979-09-01249-x.

27. Giusti, C., Pastalkova, E., Curto, C., and Itskov, V. (2015). Clique topology reveals intrinsic geometric structure in neural correlations. Proc National Acad Sci *112*, 13455–13460. https://doi.org/10.1073/pnas.1506407112.

28. Horak, D., Maletić, S., and Rajković, M. (2009). Persistent homology of complex networks. J. Stat. Mech. *2009*, P03034. https://doi.org/10.1088/1742-5468/2009/03/p03034.

29. Sizemore, A.E., Phillips-Cremins, J.E., Ghrist, R., and Bassett, D.S. (2019). The importance of the whole: Topological data analysis for the network neuroscientist. Netw. Neurosci. *3*, 656–673. https://doi.org/10.1162/netn_a_00073.

30. Kanari, L., Dłotko, P., Scolamiero, M., Levi, R., Shillcock, J., Hess, K., and Markram, H. (2018). A topological representation of branching neuronal morphologies. Neuroinformatics *16*, 3–13. https://doi.org/10.1007/s12021-017-9341-1.

31. Van Pelt, J., van Ooygen, A., and Uylings, H.B. (2001). Modeling dendritic geometry and the development of nerve connections. In Computational Neuroscience, E.D. Schutter, ed. (CRC Press), pp. 200–229.

32. Van Pelt, J., Uylings, H.B., Verwer, R.W., Pentney, R.J., and Woldenberg, M.J. (1992). Tree asymmetry—A sensitive and practical measure for binary topological trees. B Math Biol *54*, 759–784. https://doi.org/10.1007/bf02459929.

33. Strahler, A.N. (1952). Hypsometric area-altitude analysis of erosional topography. Geol. Soc. Am. Bull. *63*, 1117–1142. https://doi.org/10.1130/0016-7606(1952)63[1117:haaoet]2.0.co;2.

34. Vormberg, A., Effenberger, F., Muellerleile, J., and Cuntz, H. (2017). Universal features of dendrites through centripetal branch ordering. PLoS Comput. Biol. *13*, e1005615. https://doi.org/10.1371/journal.pcbi.1005615.

35. Berry, M., and Bradley, P.M. (1976). The application of network analysis to the study of branching patterns of large dendritic fields. Brain Res. *109*, 111–132. https://doi.org/10.1016/0006-8993(76)90383-8.

36. Scheele, C.L.G.J., Hannezo, E., Muraro, M.J., Zomer, A., Langedijk, N.S.M., van Oudenaarden, A., Simons, B.D., and van Rheenen, J. (2017). Identity and dynamics of mammary stem cells during branching morphogenesis. Nature *542*, 313–317. https://doi.org/10.1038/nature21046.

37. Snider, J., Pillai, A., and Stevens, C.F. (2010). A universal property of axonal and dendritic arbors. Neuron *66*, 45–56. https://doi.org/10.1016/j.neuron.2010.02.013.

38. Ascoli, G.A., and Krichmar, J.L. (2000). L-Neuron: a modeling tool for the efficient generation and parsimonious description of dendritic morphology. Neurocomputing *32–33*, 1003–1011.

39. Caserta, F., Stanley, H.E., Eldred, W.D., Daccord, G., Hausman, R.E., and Nittmann, J. (1990). Physical mechanisms underlying neurite outgrowth: A quantitative analysis of neuronal shape. Phys. Rev. Lett. *64*, 95–98. https://doi.org/10.1103/physrevlett.64.95.

40. Marks, W.B., and Burke, R.E. (2007). Simulation of motoneuron morphology in three dimensions. I. Building individual dendritic trees. J. Comp. Neurol. *503*, 685–700. https://doi.org/10.1002/cne.21418.

41. Jan, Y.-N., and Jan, L.Y. (2010). Branching out: mechanisms of dendritic arborization. Nat. Rev. Neurosci. *11*, 316–328. https://doi.org/10.1038/nrn2836.

42. Scheffer, L.K., Xu, C.S., Januszewski, M., Lu, Z., Takemura, S.Y., Hayworth, K.J., Huang, G.B., Shinomiya, K., Maitlin-Shepard, J., Berg, S., et al. (2020). A connectome and analysis of the adult Drosophila central brain. Elife *9*, e57443. https://doi.org/10.7554/elife.57443.

43. Ascoli, G.A., Donohue, D.E., and Halavi, M. (2007). NeuroMorpho.Org: a central resource for neuronal morphologies. J. Neurosci. *27*, 9247–9251. https://doi.org/10.1523/jneurosci.2055-07.2007.

44. Newman, M. (2005). Power laws, Pareto distributions and Zipf's law. Contemp. Phys. *46*, 323–351. https://doi.org/10.1080/00107510500052444.

45. Jagers, P. (1975). Branching Processes with Biological Applications (Wiley).

46. Kliemann, W. (1987). A stochastic dynamical model for the characterization of the geometrical structure of dendritic processes. Bull. Math. Biol. *49*, 135–152. https://doi.org/10.1007/bf02459695.

47. Hwang, R.Y., Zhong, L., Xu, Y., Johnson, T., Zhang, F., Deisseroth, K., and Tracey, W.D. (2007). Nociceptive neurons protect Drosophila larvae from parasitoid wasps. Curr. Biol. *17*, 2105–2116. https://doi.org/10.1016/j.cub.2007.11.029.

48. Hannezo, E., Scheele, C.L.G.J., Moad, M., Drogo, N., Heer, R., Sampogna, R.V., van Rheenen, J., and Simons, B.D. (2017). A unifying theory of branching morphogenesis. Cell *171*, 242–255.e27. https://doi.org/10.1016/j.cell.2017.08.026.

49. Rapp, M., Segev, I., and Yarom, Y. (1994). Physiology, morphology and detailed passive models of guinea-pig cerebellar Purkinje cells. J. Physiol. *474*, 101–118. https://doi.org/10.1113/jphysiol.1994.sp020006.

50. Anwar, H., Roome, C.J., Nedelescu, H., Chen, W., Kuhn, B., and De Schutter, E. (2014). Dendritic diameters affect the spatial variability of intracellular calcium dynamics in computer models. Front. Cell. Neurosci. *8*, 168. https://doi.org/10.3389/fncel.2014.00168.

51. Vetter, P., Roth, A., and Häusser, M. (2001). Propagation of action potentials in dendrites depends on dendritic morphology. J. Neurophysiol. *85*, 926–937. https://doi.org/10.1152/jn.2001.85.2.926.

52. Werginz, P., Raghuram, V., and Fried, S.I. (2020). The relationship between morphological properties and thresholds to extracellular electric stimulation in RGCs. J. Neural. Eng. *17*, 045015. https://doi.org/10.1088/1741-2552/abab47.

53. Kendall, W.S., Last, G., and Molchanov, I.S. (2008). New Perspectives in Stochastic Geometry. Oberwolfach Rep *5*, 2655–2702. https://doi.org/10.4171/owr/2008/47.

54. Van Pelt, J., and Verwer, R.W. (1985). Growth models (including terminal and segmental branching) for topological binary trees. Bull. Math. Biol. *47*, 323–336. https://doi.org/10.1016/s0092-8240(85)90029-1.

55. Cuntz, H., Forstner, F., Haag, J., and Borst, A. (2008). The morphological identity of insect dendrites. PLoS Comput. Biol. *4*, e1000251. https://doi.org/10.1371/journal.pcbi.1000251.

56. Nanda, S., Das, R., Bhattacharjee, S., Cox, D.N., and Ascoli, G.A. (2018). Morphological determinants of dendritic arborization neurons in Drosophila larva. Brain Struct. Funct. *223*, 1107–1120. https://doi.org/10.1007/s00429-017-1541-9.

57. Van Pelt, J. (1997). Effect of Pruning on Dendritic Tree Topology. J. Theor. Biol. *186*, 17–32. https://doi.org/10.1006/jtbi.1996.0341.

58. Grueber, W.B., Jan, L.Y., and Jan, Y.N. (2002). Tiling of the Drosophila epidermis by multidendritic sensory neurons. Development *129*, 2867–2878. https://doi.org/10.1242/dev.129.12.2867.

59. Stürner, T., Ferreira Castro, A., Philipps, M., Cuntz, H., and Tavosanis, G. (2022). The branching code: A model of actin-driven dendrite arborization. Cell Rep. *39*, 110746. https://doi.org/10.1016/j.celrep.2022.110746.

60. Van Pelt, J., and Verwer, R.W. (1986). Topological properties of binary trees grown with order-dependent branching probabilities. Bull. Math. Biol. *48*, 197–211. https://doi.org/10.1007/bf02460023.

61. Cardy, J. (1996). Scaling and Renormalization in Statistical Physics (Cambridge university press).

62. Hotulainen, P., and Hoogenraad, C.C. (2010). Actin in dendritic spines: connecting dynamics to function. J. Cell Biol. *189*, 619–629. https://doi.org/10.1083/jcb.201003008.

63. Kapitein, L.C., and Hoogenraad, C.C. (2015). Building the neuronal microtubule cytoskeleton. Neuron *87*, 492–506. https://doi.org/10.1016/j.neuron.2015.05.046.

64. Schneider, C.A., Rasband, W.S., and Eliceiri, K.W. (2012). NIH Image to ImageJ: 25 years of image analysis. Nat. Methods *9*, 671–675. https://doi.org/10.1038/nmeth.2089.

65. Han, C., Wang, D., Soba, P., Zhu, S., Lin, X., Jan, L.Y., and Jan, Y.-N. (2012). Integrins regulate repulsion-mediated dendritic patterning of Drosophila sensory neurons by restricting dendrites in a 2D space. Neuron *73*, 64–78. https://doi.org/10.1016/j.neuron.2011.10.036.

66. Smith, R.J. (2009). Use and misuse of the reduced major axis for line-fitting. Am. J. Phys. Anthropol. *140*, 476–486. https://doi.org/10.1002/ajpa.21090.

67. Warton, D.I., Wright, I.J., Falster, D.S., and Westoby, M. (2006). Bivariate line-fitting methods for allometry. Biol. Rev. *81*, 259–291. https://doi.org/10.1017/s1464793106007007.

68. Turner, N.L., Macrina, T., Bae, J.A., Yang, R., Wilson, A.M., Schneider-Mizell, C., Lee, K., Lu, R., Wu, J., Bodor, A.L., et al. (2022). Reconstruction of neocortex: Organelles, compartments, cells, circuits, and activity. Cell *185*, 1082–1100.e24. https://doi.org/10.1016/j.cell.2022.01.023.

69. Dorkenwald, S., Turner, N.L., Macrina, T., Lee, K., Lu, R., Wu, J., Bodor, A.L., Bleckert, A.A., Brittain, D., Kemnitz, N., et al. (2022). Binary and analog variation of synapses between cortical pyramidal neurons. Elife *11*, e76120. https://doi.org/10.7554/elife.76120.

STAR★METHODS

KEY RESOURCES TABLE

REAGENT or RESOURCE	SOURCE	IDENTIFIER
Experimental models: Organisms/strains		
D. melanogaster: *y[1] w[*]; PBac{y[+mDint2] w[+mC] = nompC-GAL4.P}VK00014; Df(3L)Ly, sens[Ly-1]/TM6C, Sb[1] Tb[1]*	Bloomington Drosophila Stock Center	36361
D. melanogaster: *w[1118]; P{y[+t7.7] w[+mC] = 10XUAS-IVS-mCD8::GFP}su(Hw)attP1*	Bloomington Drosophila Stock Center	32187
D. melanogaster: *ppk-cd4-tdGFP*	Chun Han, Cornell	N/A
Deposited data		
Neuron images and MICrONS dataset	This study	Mendeley Data: https://data.mendeley.com/datasets/z97bs2c8p7/1
Software and algorithms		
Code for this paper	This study	https://github.com/Maijia-cpu/Topology-properties-of-neurons/tree/main
TREES toolbox	Cuntz et al.[13]	https://www.treestoolbox.org/
MATLAB	Version R2021a	https://se.mathworks.com/products/matlab.html
ImageJ	Schneider et al.[64]	https://imagej.net
GraphPad Prism	Version 08	https://www.graphpad.com/

RESOURCE AVAILABILITY

Lead contact

Further information and requests for resources and reagents should be directed to and will be fulfilled by the Lead Contact, Jonathon Howard (joe.howard@yale.edu).

Materials availability

This study did not generate new unique reagents.

Data and code availability

- All data reported in the paper have been deposited at Mendeley and are publicly available. DOIs are listed in the Key resources table.
- All original code has been deposited at Github and is publicly available. Link is provided in the Key resources table.
- Any additional information required to reanalyze the data reported in this paper is available from the Lead Contact upon request.

EXPERIMENTAL MODEL AND SUBJECT DETAILS

Drosophila melanogaster strains

Drosophila melanogaster larvae were raised on cornmeal-agar medium with glucose and yeast (Glucose D2, Archon Scientific) at 25 °C. 96hr AEL larvae were used for all analyses. For visualization of dendritic morphologies of class III neurons (ddaF), *nompC-Gal4* (Stock 36361 from Bloomington *Drosophila* Stock Center) was crossed with 10XUAS-mCD8GFP (32187). The fly strain *ppk-cd4-tdGFP* (a gift from Han Chun (Cornell University)) was used for imaging class IV neurons.

METHOD DETAILS

Scale invariance and power laws

We say that a function, $f(x)$, is scale invariant if changing the scale or units of x leaves the shape of f unchanged (except for a multiplicative constant). In other words, $f(\lambda x) = g(\lambda)f(x)$ (Equation 1) where the function g does not depend on x. This is sometimes called scale-free, but we use the term scale invariance. Because $f(\lambda_1\lambda_2 x) = g(\lambda_1\lambda_2)f(x) = g(\lambda_1)f(\lambda_2 x) = g(\lambda_1)g(\lambda_2)f(x)$, we must

have $g(\lambda_1\lambda_2) = g(\lambda_1)g(\lambda_2)$ (provided f is non-zero). By Cauchy's multiplicative function equation, $g(\lambda)$ is of the form $g(\lambda) = \lambda^{-\alpha}$, where α is a constant. Substituting $x = 1$ into Equation 1 gives $f(\lambda) = g(\lambda)f(1)$. After substituting $\lambda = x$, the required power law follows: $f(x) = f(1)g(x) = f(1)x^{-\alpha}$. This function is linear when plotted on log axes because $\ln f(x) = \ln f(1) - \alpha \ln x$. The log-log slope is $-\alpha$. It is easy to show the converse is also true: a power law implies scale invariance.

Spinning disk confocal imaging

Embryos were collected for 2 h on apple juice agar plates with a dollop of yeast paste and aged at 25°C in a moist chamber. The plates containing the first batch of embryos were discarded as the dendrite morphology of sensory neurons is less consistent in those animals.[65] Larvae were immobilized individually on agarose pads (thickness 0.3–0.5mm) sandwiched between a slide and a coverslip. The imaging was done using a spinning disk microscope: the Yokogawa CSU-W1 disk (pinhole size 50 μm) built on a fully automated Nikon TI inverted microscope with perfect focus system, an sCMOS camera (Zyla 4.2 plus sCMOS), and running Nikon Elements software. Individual neuron image stacks were acquired with a 60 × 1.2 NA water immersion lens with a z step size 0.16 μm.

Data processing method

To reveal the power-law form of the density distribution it is better to plot the density histogram on logarithmic scales. However, the right-hand end of the distribution is noisy because of sampling errors. To deal with it, we vary the width of the bins in the density histogram and normalize the sample counts by the width of the bins they fall in. That is, the number of samples (denoted by $\sum_n^{n+\Delta n} N(n)$) in a bin of width Δn should be divided by Δn to get a count per interval of n (i.e., average count denoted by M). Note that we only consider sample counts larger than 10 to reduce the statistical error. The standard deviation of the normalized count is calculated as: $\sqrt{\sum_n^{n+\Delta n} N(n)+2}/\Delta n$. Then the normalized sample count becomes independent of bin width on average and we are free to vary the bin widths as we like. Here we use *logarithmic binning*.[44] We choose a multiplier of 2 and create bins that span the intervals 1.5 to 2.5, 2.5 to 4.5, 4.5 to 8.5 and so forth. The first point $N(1)$, which is just the total number of leaves (or tips), is neglected in the fitting unless the maximal tip number is less than 60 or the total number of normalized sample count is less than 5. The normalized sample counts and the center of the bins are used to plot the results.

Reduced major axis (RMA) linear regression method

In our manuscript, the power law exponent α is obtained using reduced major axis (RMA) linear regression on the log-log transformed data. RMA regression[66,67] is often recommended in allometric scaling analysis when it is difficult to establish a cause-effect relationship between the variables x and y. In simple linear regression, it is assumed that y depends on x with additive noise: the slope is $b_{xy} = r_{xy}s_{xy}/s_x^2$, where r_{xy} is the Pearson correlation coefficient, s_{xy} is the sample cross-correlation and s_x^2 is the sample variance in x. The RMA slope is the geometrical mean of the two slopes obtained by simple linear regression: b_{xy} (y the dependent variable) and b_{yx} (x the dependent variable): $b_{\mathrm{RMA}} = \mathrm{sign}(r_{xy})\sqrt{b_{xy}/b_{y,x}} = \mathrm{sign}(r_{xy})\frac{\sigma_y}{\sigma_x}$.

Perfection index calculation

A function *perfection_tree* is made available as part of the TREES Toolbox[13] in MATLAB and Github.

Bifurcation probability measurement from experimentally reconstructed neurons

All branches of a reconstructed neuron were classified according to their branch orders d. Within each branch order, the number n of branches that bifurcate further (generate two daughter branches) was counted. The bifurcation probability at each branch order is defined as the ratio between n and the total number m of branches within that branch order. To obtain enough statistics, only branch orders with total branch number m larger than 6 were used for bifurcation probability calculation.

Methods for MICrONS dataset analysis

Spine data were recovered from an electron microscopy dataset on layer 2/3 of the mouse visual cortex generated by the MICrONS program. 301 publicly available neuron reconstructions without spines[68] were cross-referenced with ~3.2 million automatically identified synapses from the same volume.[69] As the synapse dataset is known to contain false-positives, synapses that would imply a spine length of greater than 4 μm were excluded from our analysis.

Simulating trees with balancing factors

In the functional simulations, the synthetic tree is constrained by the "density profile" of a neuron group and by a balancing factor (*bf*)[13] that weighs two demands: the minimization of resources and the minimization of conduction time. Higher *bf* values correspond to increased importance of conduction time minimization relative to resource minimization and vice versa. The simulation was carried out using the TREES Toolbox package in the MATLAB environment. 3000 random points were generated and synthetic trees starting at the center point according to the balancing factor from 0 to 1 in the step of 0.1 were created for further analyses. For each balancing factor, 100 synthetic trees were created. Note that there exist only two $N(n)$ values when balancing factor is set to 1. Thus, the tree perfection index for $bf = 1$ is not calculated in Figure 6B.

Cell Reports, Volume *42*

Supplemental information

Topology recapitulates morphogenesis of neuronal dendrites

Maijia Liao, Alex D. Bird, Hermann Cuntz, and Jonathon Howard

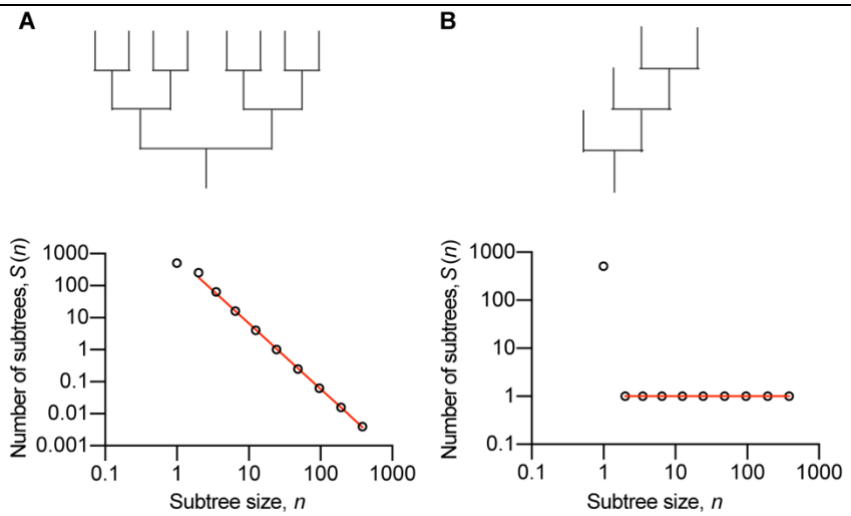

Figure S1. Perfection indices of perfect and imperfect trees. A A perfect tree is shown above (bifurcation probability $p = 1$). The number of subtrees with size n (n defined as the number of tips) is plotted against n with log-log axes. The points fall on a line: $S(n) = n_{\mathrm{tot}} n^{-\alpha}$ (n_{tot} is the total number of tips). The perfection index is defined $\beta = \alpha/2 = 1.04 \pm 0.02 \cong 1$ when fit using reduced major axis (RMA) linear regression (See STAR Methods). **B** A maximally imperfect tree is shown above (one tip produced at each bifurcation). The log-log slope is zero (omitting the first point). The perfection index is therefore 0.

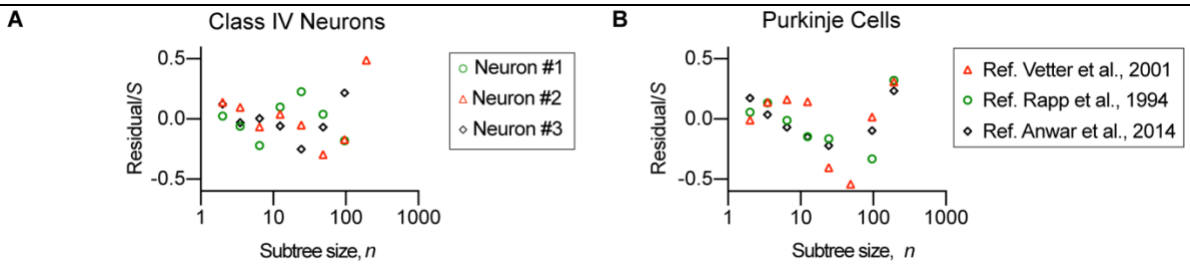

Figure S2. Residual plots confirm the goodness of fit using reduced major axis (RMA) linear regression. A. Normalized residuals for the RMA fit to the log-log plot of the subtree size distribution ($[S(n) - S_{\mathrm{fit}}(n)]/(S(n)$, where S is the subtree site and S_{fit} is the RMA fit) for class IV cells. **B**. Same for Purkinje cells.

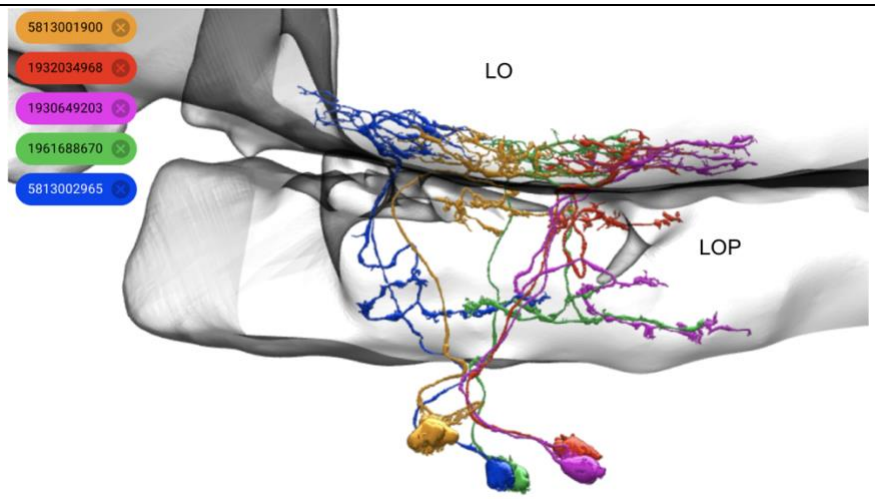

Figure S3. Five examples of T5 cells from the adult fly central nervous system. Five motion-sensitive T5 cells have dendrites in the lobula (LO) and axons in the lobula plate (LOP) (from the Hemibrain dataset). The identification numbers are indicated at the upper left.

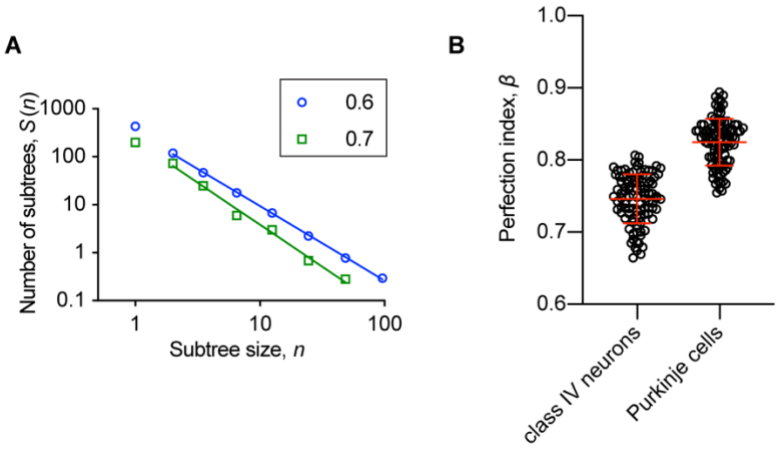

Figure S4. Trees generated by the Galton-Watson process follow power laws. A. Trees generated using bifurcation probabilities of 0.6 and 0.7, which are above the percolation threshold of 0.5, follow power laws with perfection indices equal to 0.78 and 0.88 respectively. **B.** Galton-Watson simulations using the experimentally measured bifurcation probabilities from class IV neurons (Fig. 5A) and Purkinje cells (Fig. 5D) follow lower laws with perfection indices of 0.75 ± 0.03 (mean ± SD, N = 100 simulations) and 0.82 ± 0.03 (mean ± SD, N=100) respectively. The indices from the simulations are close to those measured from the original data (0.70 and 0.86 respectively).

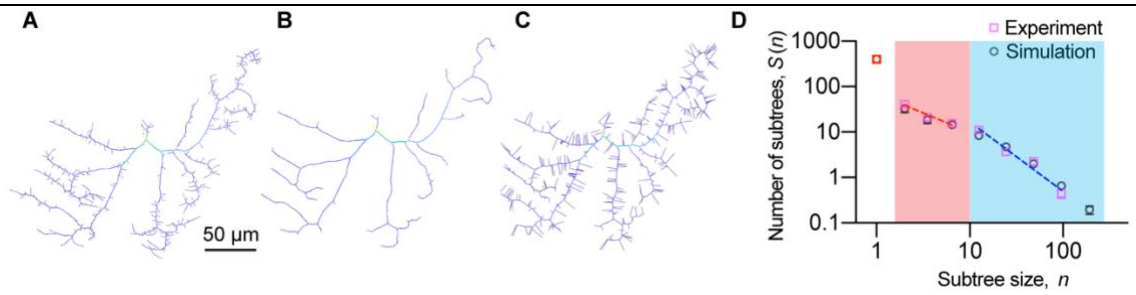

Figure S5. Simulations show that branchlets lead to two-phase scaling. A A class III neuron. **B** The same cell with its 363 terminal branchlets removed. **C** 363 terminal branches with average length 10µm were added back at random positions on the trimmed backbone. **D** Comparison of the subtree-size distributions for the neurons in A and C (Figure 7B in main text). The random addition of terminal branches recapitulates the two-phase behavior measured from experimental data. The dashed lines represent the slopes in the two regions.

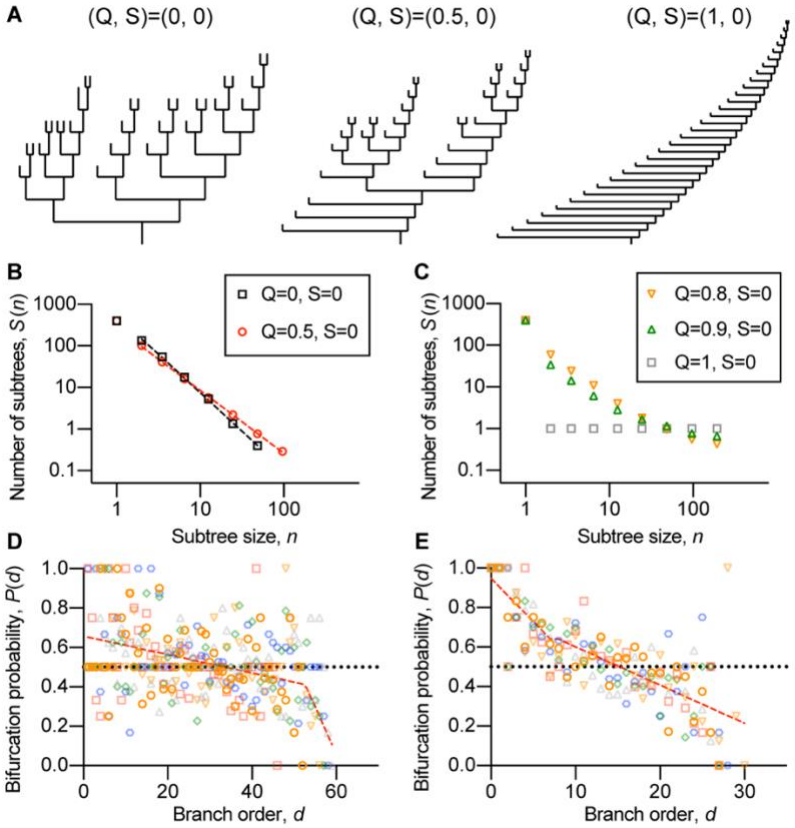

Figure S6. Trees generated by the QS model with different ratios of internal-to-tip branching. A. Trees generated with (Q,S) = (0,0) (no internal branching), (Q,S) = (0.5,0) (equal internal and tip branching), and (Q,S) = (1,0) (all internal branching). **B.** Subtree-size distributions with QS values (0,0) and (0.5,0). The respective perfection indices are 0.93 and 0.76. Average of 20 simulations. **C.** Subtree-size distributions with QS values (0.8,0), (0.9,0), and (1,0). Average of 20 simulations. Note that the (0.8,0) and (0.9,0) curves are concave. **D,E** Bifurcation probabilities, $P(d)$, as a function of branch order, d, with QS values (0.5,0) and (0.2,0) respectively. Different colors represent six different simulations. Linear piecewise fits (dashed red lines) are overlaid. The bifurcation probabilities for orders less than or equal to 10 are 0.62 ± 0.02 (mean ± SD, *N*=6 simulations) for QS values (0.5,0) and 0.70 ± 0.02 (mean ± SD, *N*=6 simulations) for QS values (0.2,0).